Computational Analysis of Orthogonal Blade Vortex Interaction

Antonio Filippone*
The University of Manchester
Manchester M60 1QD

Abstract

This contribution reviews the research in orthogonal blade vortex interaction (OBVI) and presents some results of computational simulation with the unsteady Reynolds-averaged Navier-Stokes equations with turbulence closure equations. The cases investigated are relative to a subcritical interaction between a lifting blade at a high angle of attack and an orthogonal vortex that travels either head-on or at 45 degrees to the leading edge. The numerical simulations have been performed at a Reynolds number $Re = 1.85 \cdot 10^5$ and a vortex Reynolds number $Re_v = 10^5$. A comparison between the case of straight and oblique BVI indicates that the blade-vortex interaction pressure peak is less severe in the latter case. The lift and drag coefficients peak at different positions of the vortex.

1 Introduction

The interaction between a vortex and a blade is a common occurrence in helicopter aerodynamics. Several mechanisms have been identified in the past[1]. One of these is the interaction between a main-blade tip vortex and an incoming blade. Another case is the interaction between a main-blade tip vortex and a tail rotor blade. The interaction consists either in a vortex flying past a blade in a near encounter, or in a vortex being cut by the incoming blade. This paper addresses specifically the problem of vortex cutting. Even on first analysis, there is a substantial difference between the two cases. In fact, vortex cutting causes the blade to pass through a layer of vorticity. This type of BVI is stronger, and and is known to give rise to impulsive blade loads, structural vibrations and noise emission. When the axis of the vortex is normal to the axis of the blade, the case is called orthogonal blade vortex interaction (OBVI). However, the flight path of the vortex can be arbitrary, because it depends on the actual position of a rotating blade with respect to a vortex flight path that is almost linear. For this reason, two basic cases are considered in the present analysis. In the first case the orthogonal vortex travels head-on against the blade; in the second case the vortex travels at 45 degrees with the axis of the blade, as shown in Fig. 1.

In the present context, the main parameters of the interaction are: the relative speed between vortex and blade; size of the vortex core relatively to the blade thickness; the blade's relative thickness, the axial velocity component of the vortex and the circulation of the vortex. Other parameters are the angle of attack (or the lift coefficient) of the blade and the flight direction of the vortex with respect to the blade. Some of these parameters form a consistent group of dimensionless quantities.

*School of MACE, George Begg Building, E-mail: a.filippone@manchester.ac.uk; telephone: +44 – 161 – 306 3702 (direct)

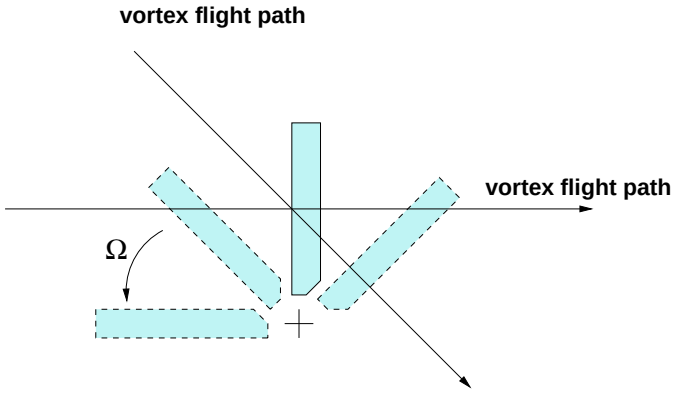

Figure 1: *Vortex flight paths in orthogonal BVI.*

Dimensionless parameters are essential in the rational investigation the fluid dynamic effects of the vortex interaction, as discussed and demonstrated by Krishnamoorthy & Marshall[2].

A considerable amount of the research available on BVI addresses aeroacoustic problems. This is natural, since the acoustic emission is the most evident and annoying effect of a BVI. Another unwanted effect is the so-called blade slap. A review of state of the art of the orthogonal BVI was published by Coton et al.[3], who reported both the experimental and computational results available. Considerable experimental work has been carried out by the aerodynamics group at Glasgow University[8;9;10;11]. In particular, Green *et al.*[11] performed stereo particle-image velocimmetry (PIV) experiments to highlight the three-dimensional nature of the vortex interaction and provided detailed pictures of the vorticity on the upper and lower surface of the blade. Previous computational analysis on the the orthogonal BVI include the work of Marshall *et al.*[5;6;7]. Other vortex interactions exist. It is worth mentioning the effects of a vortex impacting onto a non lifting surface and the interaction between a strong vortex and the wake of a lifting blade[12;13].

The present research addresses a novel aspect, that is the transient aerodynamic response of a lifting tail rotor blade and the analysis of the vortex dynamics. In a previous study[4], the author addressed the role of some dimensionless parameters for various BVI cases.

2 Non Dimensional Parameters

Consider a vortex with circulation Λ and vortex core σ_o travelling with a speed U_∞. This vortex has an axial speed w_o at its centre. The distribution of axial velocity has been investigated experimentally by Bhagwat & Leishman[14]. The thickness parameter is the ratio between the blade thickness t and the radius of the vortex core σ_o

$$\tau = t/\sigma_o \tag{1}$$

the impact parameter

$$I = 2\pi\sigma_o U_\infty/\Gamma \tag{2}$$

which is the ratio between the relative impact speed and the swirl velocity. The the axial flow parameter A is the ratio between the axial velocity and the swirl velocity:

$$A = 2\pi\sigma_o w_o/\Gamma \tag{3}$$

Finally, there is the vortex-based Reynolds number, $Re_v = \Gamma/\nu$. Marshall & Krishnamoorthy[6] identified two distinct phases in the BVI interaction, depending on the value of the impact parameter and the thickness parameter. For a thickness parameter $t/\sigma_o < 1$ (which is typical of helicopter problems), if the impact parameter $I > 0.25$ the interaction is weak, and the boundary layer remains attached before and during the BVI, except in local spots. If $I < 0.1$, the strength of the vortex causes a suction of the boundary layer *before* the blade cuts the vortex. This type of interaction (called supercritical) is even more disruptive. In the intermediate values of the impact factor, there is a transition region. As shown in Ref.[4], the application considered leads to an impact factor $I > 1$ with $t/\sigma_o \simeq 0.2$; this leads to a sufficiently weak OBVI case.

3 Computational Model

The computational model consists of an unsteady Reynolds-averaged Navier-Stokes code. The computational model was the open-source `Code Saturne`, with Menter's shear-stress turbulence model[15]. The integration domain and the relevant boundary conditions are shown in Fig. 2. The plane $x - y$ is normal to the blade section; the third axis z runs along the span and makes a right-hand system with x and y. Periodic boundary conditions have been used on the sides of the domain and on the upper and lower walls. The boundary conditions are closed with an inlet (convective speed) and an outlet, downstream the blade. Particular care is needed in setting initial conditions that define the orthogonal vortex. The problem was solved iteratively, by assigning a value of the circulation and calculating the field of swirl velocity.

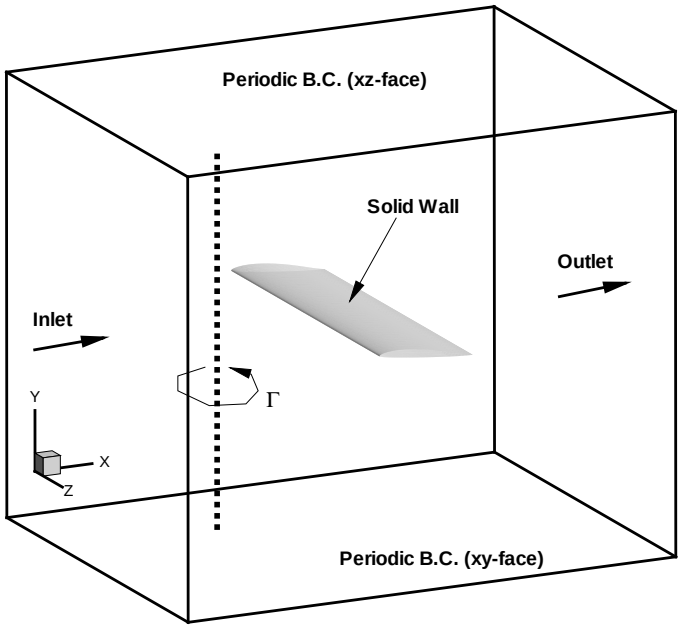

Figure 2: *Integration domain and boundary conditions.*

A structured grid that forms a rectangular box around the blade was used, as shown in Fig. 3. The fine mesh size was about 1.76 million cells.

The blade section was the S102E airfoil, set at an angle of incidence of 9 degrees. The chord was 0.074 m. The convecting speed of the vortex was 36 m/s, corresponding to a Reynolds number $Re = 1.85 \cdot 10^5$ and a vortex Reynolds number $Re_v = 10^5$. Furthermore, the vortex circulation was set to $\Gamma = 4.5$. The vortex flight path did not have an axial component; therefore, the axial velocity factor was negligible, though non zero, due to self-induced velocity

during the interaction. The time-step was 10^{-4} seconds. The average CFL number is 1.5, based on time-step and grid resolution.

The problem was run in stages. First, a steady-state solution was achieved in absence of the vortex. Then the vortex condition was added and the solution was restarted in unsteady mode with the vortex convected downstream in the specified direction.

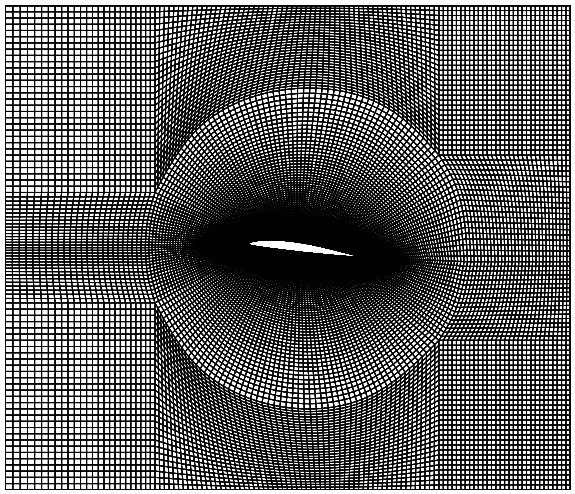

Figure 3: *Mesh details on a blade section.*

The initial axial velocity of the vortex is zero, but as the vortex travels a self-induced velocity causes the vortex to move axially well before the impact on the blade. The analysis is carried out on the vortex dynamics and on the blade aerodynamics. The data investigated include the behaviour of the pressure field as the vortex advances, the distribution of vorticity, the interaction of the vortex with the blade and the wake, the flow separation at the blade surface and the path lines of the flow.

4 Results and Discussion

The analysis was carried out to examine the unsteady aerodynamic response caused by a subcritical OBVI. Also, a detailed analysis of the vortex dynamics has been done.

4.1 Vortex Dynamics

Figure 4 shows some time-frames of the vortex dynamics as the vortex approaches the blade in a head-on interaction. In particular, Fig. 4a shows the vortex before the interaction. The data visualised is an iso-vorticity level. A pressure wave is seen to propagate from the interaction point. It is possible that this wave is a result of the outer boundary conditions, but this event could not be evaluated more rationally, as it required the problem to be resolved with a smaller time step and with variable grid size. In any case, the vortex is well defined and is cut by the blade as shown in Fig. 4b. Unlike inviscid vortices, the present case shows that the vortex is indeed cut and that there is not a full reconnection at the trailing edge, due to the different convective speed of the vortex.

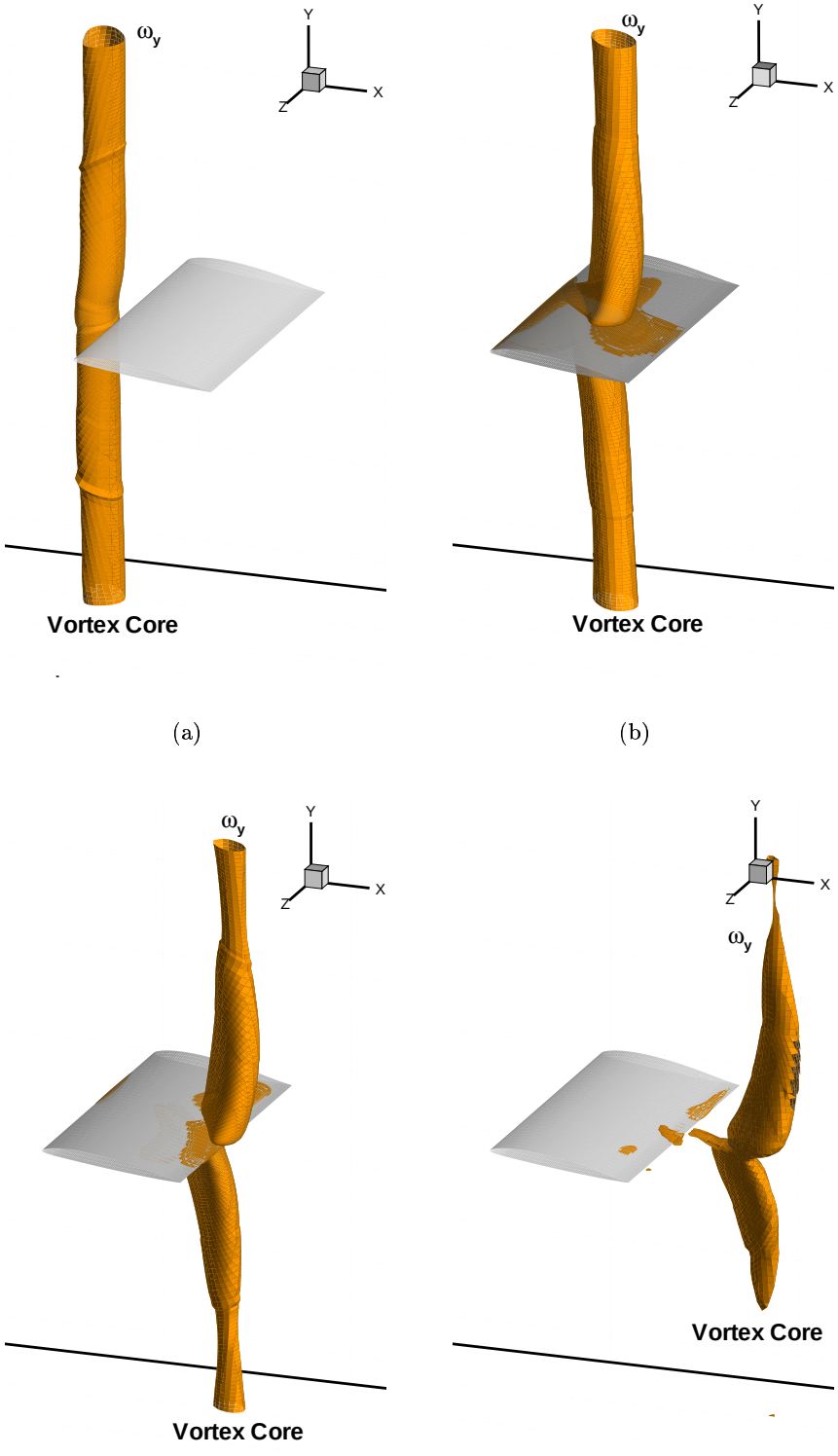

Figure 4: *Vortex interaction on the straight orthogonal BVI.*

This is due to the fact that the two vortices, once separated at the leading edge, are convected with a different speed. A finer resolution is required to resolve the full extent of the interaction between the wake and the vortex.

A similar analysis has been carried out for the oblique interaction. This is shown in Fig. 5. In this case, the vortex undergoes a cross-wise stretching at the wing surface and tends to dissipate faster than the BVI with a normal impact. Note that the is a layer of relatively strong vorticity across the leading edge of the blade.

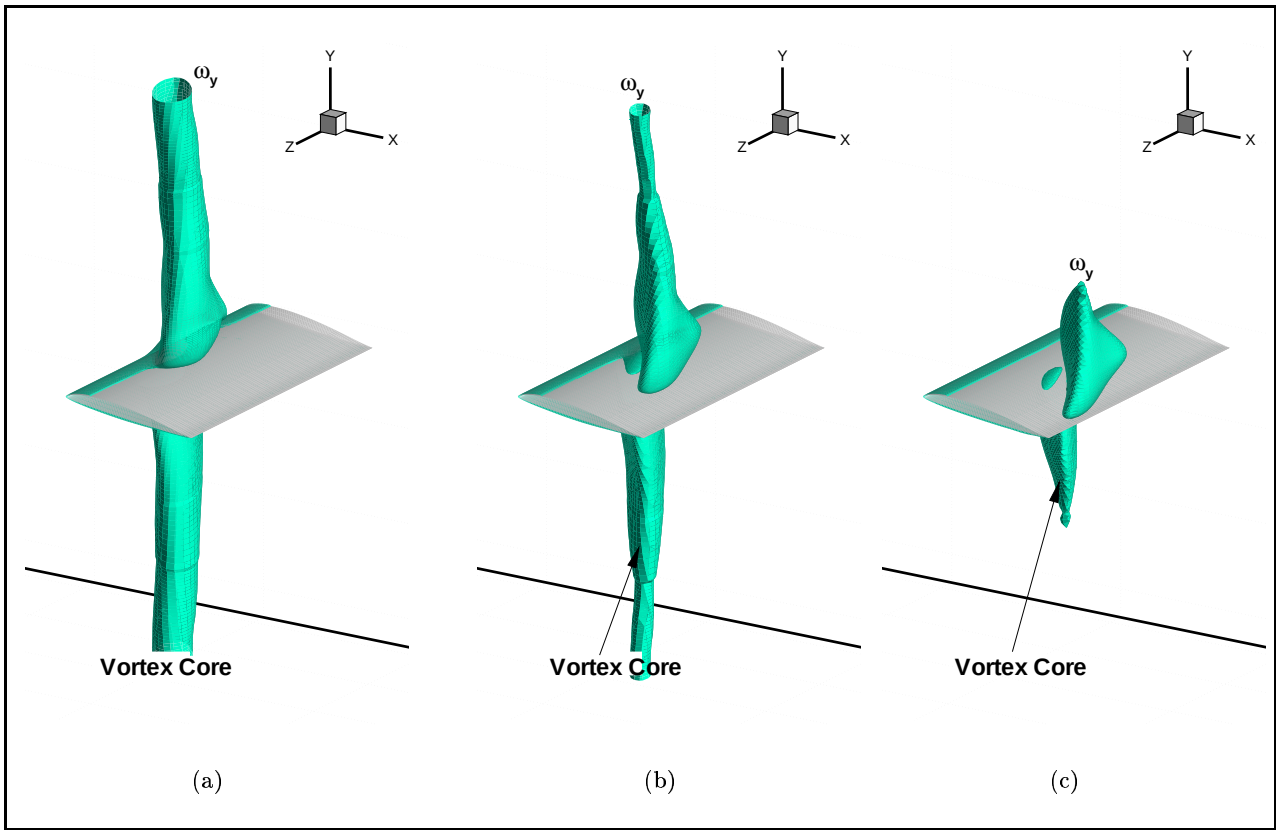

Figure 5: *Vortex interaction on the oblique BVI.*

The three-dimensional effects are more evident when we analyse the position of the vortex core on a plane normal to the axis of the blade, e.g. on a constant$-x$ plane. This effect is shown in Fig. 6. This case refers to a time when both vortices have departed from the trailing edge. Figure 6a shows an iso-vorticity level on a plane normal to the leading edge passing through the centre of the upper vortex; Fig 6b is similar, but the cut is taken through the centre of the lower vortex. One of the notable effects of the interaction is the spanwise deformation of the vortex axis, that appears inclined to the right. The axis itself appears to be wavy.

It is also of some interest to map the position of the vortex core as the upper and lower vortices travel through the blade. The problem with this tracking is that the vortex is stretched both in the axial and in the spanwise direction. Thus, we decided to chose some points along the axis of the vortex that are at a fixed distance from the wall. This distance is normalised with the chord. Figure 7 shows such a flight path. When the vortex is cut by the blade, we note that their path is different. When the upper vortex is around the trailing edge (point A), the lower vortex has travelled past to point B. The two vortices *do not* reconnect at the trailing edge, because they travel in different directions with a different convective speed. The data shown in Fig. 7 refer to two positions above the blade's surface, $y/c = 1/8$ and $y/c = 1/4$.

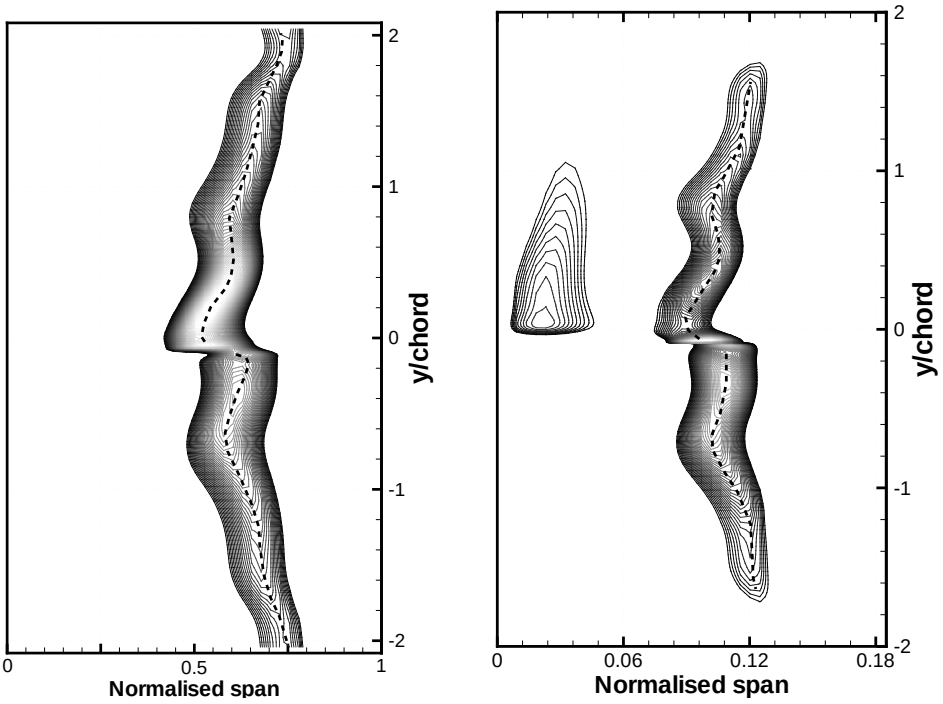

(a) (b)

Figure 6: *Front view of vortex core during an oblique OBVI.*

4.2 Analysis of Aerodynamic Forces

Figure 8 shows the time-dependent aerodynamic coefficients for both impact cases. The data plotted are the net change over the steady state case (before the impact takes place). Predictably, after the vortex has passed, the net effect is zero. However, the forces are impulsive. From the analysis of the absolute values of the coefficient, we found that the C_L increases by about 15% for the straight OBVI, and by about 11% for the oblique OBVI. The C_D by about 23% and 24%, respectively. The position of the vortex corresponding to the peak in the aerodynamic coefficients is indicated in the graphs. In particular, it is noted that the direction of the flight path does not affect the peak in the C_D; this is not the case for the C_L, whose peak is delayed by the change in flight direction.

As mentioned, a comparison with the experimental data for a real-case BVI on a helicopter tail rotor is somewhat difficult, because the experiments inevitably contain complications (geometrical and otherwise) that is difficult to replicate in a simulation model. An example is shown in the case of the basic experiment performed by Wang *et al.*[16], Fig. 9. In this experiment, a rotating blade cuts an incoming vortex generated by an oscillating rectangular wing placed upstream. The data indicate that before the interaction has subsided the blade has moved away from the vortex. This would explain why the normal force data seem incomplete. In other words, once the vortex has travelled past the blade (or vice versa), the net effect on the aerodynamic coefficient should be zero, as indicated also in the results of Fig. 8. A relatively high level of turbulence is present in these experimental data. The differential normal force coefficient, C_n, depends on the impact velocity. However, it is not possible to assess at what angle the blade cuts the vortex.

A comparison is done between two sets of experimental data (at the velocities indicated)

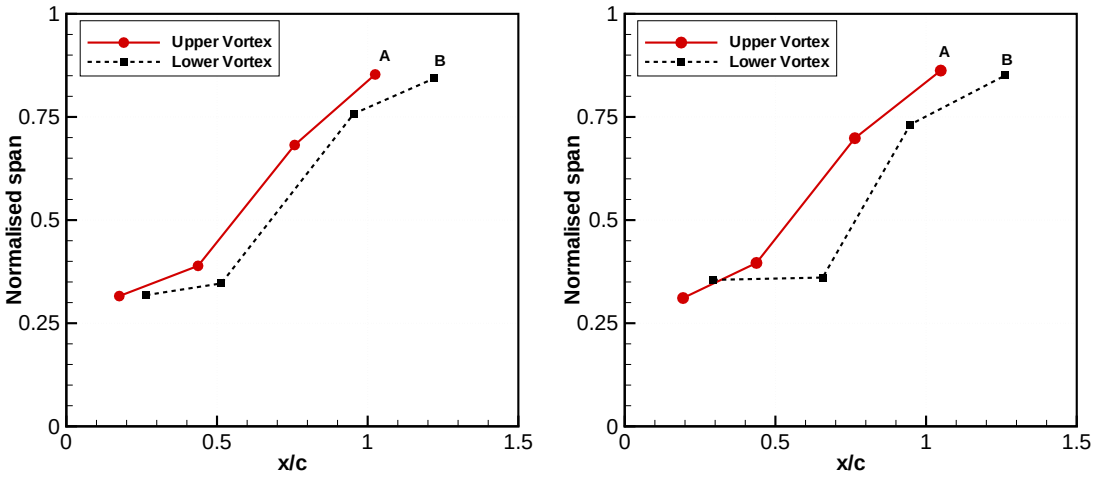

(a) $y/c = 1/8$ (b) $y/c = 1/4$

Figure 7: *Vortex core path in oblique BVI at selected distances from from blade surface.*

and the present computations for both impact directions. Once the aerodynamic forces and the flow time are normalised, the peak in C_n is well captured for the straight OBVI at a speed of 40 m/s, but not at a speed of 30 m/s. As noted, the calculations were carried out at an intermediate velocity of about 36 m/s. Another aspect that must be pointed out is the loss in normal force at the lower speed prior to the impact. However, both in the computed data and in the wind tunnel data at 40 m/s there seems to be more turbulent effect that effective loss of normal force.

5 Conclusions

The orthogonal blade-vortex interaction has been simulated with a computational method under realistic conditions for a helicopter tail rotor environment. This included the case of a lifting blade at turbulent Reynolds numbers, and a vortex flight path along two different directions. The results show an impulsive response of the surface pressure and the aerodynamic coefficients. Once the vortex has travelled past the blade, the aerodynamic loading is restored to the conditions before the interaction.

The fluid dynamic analysis has revealed the complexity of the interaction, which is in all cases strongly three-dimensional. In particular, when the vortex impacts the blade along an oblique flight path, it is cut into two separate vortices that travel along different directions and fail to reconnect at the trailing edge. In case of an oblique interaction there is a stronger deformation of the core near the surface.

Comparisons with some experimental data have been shown. The results highlighted the difference in flow condition between the computational model and the experimental setup. Although the impulsive rise in the normal force coefficient is approximately predicted, the peak of the coefficient is not. Furthermore, the experimental data appear to be an incomplete series; this highlights the difficulty of the interaction process.

Improvements are required in the boundary conditions. In particular, a detailed analysis is required to set the starting conditions on the vortex (distribution of axial velocity, size of

the vortex core, etc.). Further investigation is required to identify spurious sources of error, due to the self-induced vortex velocity on the outer boundary conditions, which has not been accounted for, and the role of the distance between the vortex and the outer boundaries.

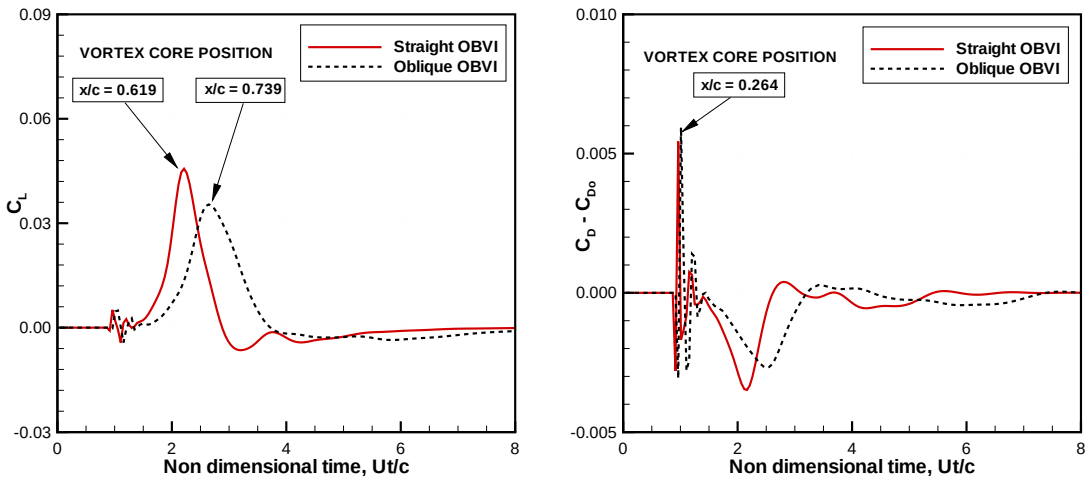

(a) C_L (b) C_D

Figure 8: *Time-dependent aerodynamic coefficients*

References

[1] Leverton JW, Pollard JS, and Wills OR. Main rotor wake/tail rotor interaction. *Vertica*, 1, pp. 213–221, 1977.

[2] Krishnamoorthy S and Marshall JS. Three-dimensional blade-vortex interaction in the strong vortex regime. *Physics of Fluids*, 10(11), pp. 2828–2845, Nov. 1998.

[3] Coton F, Marshall J, Galbraith R, and Green R. Helicopter tail rotor blade vortex interaction. *Progress in Aerospace Sciences*, 40(7), pp. 453–486, 2004.

[4] Filippone A and Afgan I. Orthogonal blade vortex interaction on a helicopter tail rotor. *AIAA Journal*, 2008.

[5] Liu X and Marshall JS. Blade penetration into a vortex core with and without axial flow. *J. Fluid Mechanics*, 519, pp. 81–103, 2004.

[6] Marshall JS and Krishnamoorthy S. On the instantaneous cutting of a columnar vortex with a non-zero axial flow. *J. Fluid Mechanics*, 351, pp. 41–74, 1997.

[7] Marshall JS and Grant JR. Penetration of a blade into a vortex core, pp. Vorticity response and unsteady blade forces. *J. Fluid Mechanics*, 306, pp. 83–109, 1996.

[8] Doolan CJ, Coton FN, and Galbraith RA. Surface pressure measurements of the orthogonal blade vortex interaction. *AIAA J.*, 38(1), pp. 88–95, 2001.

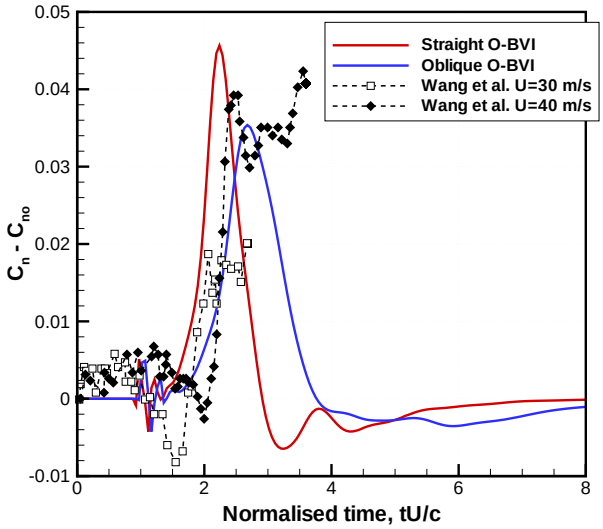

Figure 9: *Present calculations and comparison with the wind tunnel data of Wang et al.*[16].

[9] Doolan C, Coton FN, and Galbraith RA. Three-dimensional vortex interactions with a stationary blade. *Aeronautical J.*, 103(1030), pp. 579–587, 1999.

[10] Green RB, Doolan CJ, and Cannon RM. Measurements of the orthogonal blade-vortex interaction using a particle image velocimmetry technique. *Experiments in Fluids*, 29, pp. 369–379, 2000.

[11] Green RB, Coton FN, and Early JM. On the three-dimensional nature of the orthogonal blade-vortex interaction. *Experiments in Fluids*, 41, pp. 749–761, 2006.

[12] Wittmer KS, Devenport WJ, Rife MC, and Glegg SA. Perpendicular blade vortex interaction. *AIAA J.*, 33(9), pp. 1667–1674, Sept. 1995.

[13] Wittmer KS and Devenport WJ. Effects of perpendicular blade vortex interaction. Part 1, pp. Turbulence structure and development. *AIAA J.*, 37(7), pp. 805–812, July 1999.

[14] Bhagwat MJ and Leishman JG. Generalized viscous vortex model for application to free-vortex wake and aeroacoustic calculations. In *Proceedings of the 58th AHS Forum*, Montreal, June 2002.

[15] Menter F. Two-equation eddy-viscosity turbulence models for engineering applications. *AIAA J.*, 32(8), pp. 1598–1605, Aug. 1994.

[16] Wang T, Doolan CJ, Coton FN, and Galbraith RA. Experimental study of the three-dimensionality of orthogonal blade-vortex interaction. *AIAA J.*, 40(10), pp. 2037–2046, 2002.